Lithos 228–229 (2015) 12–22

Contents lists available at ScienceDirect

Lithos

journal homepage: www.elsevier.com/locate/lithos

Rare earth elements in apatite as a monitor of magmatic and metasomatic processes: The Ilímaussaq complex, South Greenland

Aurelia L.K. Zirner [a,b,*], Michael A.W. Marks [a], Thomas Wenzel [a], Dorrit E. Jacob [c,d], Gregor Markl [a]

[a] Universität Tübingen, FB Geowissenschaften, Wilhelmstrasse 56, 72074 Tübingen, Germany
[b] Universität Bonn, Steinmann-Institut für Geologie, Mineralogie und Paläontologie, Poppelsdorfer Schloss, 53115 Bonn, Germany
[c] Universität Mainz, Institut für Geowissenschaften, Petrologie, J.-J.-Becher-Weg 21, 55099 Mainz, Germany
[d] Macquarie University, Department of Earth and Planetary Sciences, North Ryde, NSW 2109, Australia

ARTICLE INFO

Article history:
Received 29 June 2014
Accepted 19 April 2015
Available online 26 April 2015

Keywords:
Ilímaussaq
Apatite
Rare earth elements
Alkaline to peralkaline rocks

ABSTRACT

Textural and compositional variations of apatite from the plutonic Ilímaussaq complex in South Greenland and its surrounding country rocks track magmatic and metasomatic processes. Detailed back-scattered electron (BSE) imaging reveals various types of apatite textures including (i) growth zonation (concentric, oscillatory as well as sector zonation) formed during magmatic differentiation, (ii) resorption and overgrowth textures due to fluid/melt induced metasomatic overprint of precursor apatite and (iii) replacement textures indicating the destabilization of apatite in favor of monazite.

In the least evolved rocks of the Ilímaussaq complex, apatite incorporates rare earth elements and Y (REY) mainly via the coupled substitution $Ca^{2+} + P^{5+} = REY^{3+} + Si^{4+}$. In the more evolved peralkaline rocks and in metasomatically overprinted rocks, however, the coupled substitution $2\ Ca^{2+} = REY^{3+} + Na^{+}$ becomes increasingly relevant, and apatite incorporates successively more LREE compared to HREE as shown by increasing $(La/Gd)_N$ and $(Gd/Yb)_N$ ratios. Similarly, at the contact between the Ilímaussaq rocks and the granitic country rocks, the metasomatic effect of the emplacement of the Ilímaussaq melts is preserved in partly resorbed precursor apatite, which is overgrown by REY-enriched apatite with higher $(La/Gd)_N$ and $(Gd/Yb)_N$ ratios compared to apatite from granites more distant from the contact.

This study shows, that apatite textures and compositions are suitable to track both primary magmatic and later fluid-present metasomatic processes. The incorporation of REY in apatite is not only dependent on the amount of REY present but also depends largely on Na activity in the apatite-precipitating melts and fluids.

© 2015 Published by Elsevier B.V.

1. Introduction

Apatite is a very common accessory mineral in most igneous rocks (Piccoli and Candela, 2002). It can incorporate halogens, S and a large range of trace metals such as Sr, Fe, Mn, U, Th, as well as the rare earth elements and Y (REY), and is a sensitive recorder of magmatic and hydrothermal processes (e.g., Harlov and Förster, 2003; Larsen, 1979; Pan and Fleet, 2002; Rønsbo, 1989, 2008; Wang et al., 2014; Watson and Green, 1981).

Based on crystallographic and chemical similarities, the apatite supergroup covers minerals with the structural formula $^{IX}M1_2^{VII}M2_3(^{IV}TO_4)_3X$. This includes phosphates, arsenates, vanadates, sulfates, and silicates, which are known to show extensive partial solid solution between end members (Pasero et al., 2010). In most igneous apatites, the X site is mainly occupied by OH, F, and Cl, the T site is largely dominated by P, and Ca is the major cation on the M sites (Piccoli and Candela, 2002). However, two structurally different M sites exist, where Ca is 9- and 7-fold coordinated as $Ca1O_9$ and $Ca2O_6X$ polyhedrons, respectively (Elliott et al., 2002; Hughes and Rakovan, 2002). Commonly, REY substitute for Ca and britholite $[(REY,Ca)_5(SiO_4)_3(OH,F)]$ represents a silicate end member that reflects the coupled substitution of Ca and P by REY and Si in the apatite structure. For various reasons, REY favor the higher coordinated Ca1 over the Ca2 site. Because of a decrease of site-occupancy ratios (REY-Ca2/REY-Ca1) with increasing atomic number, the Ca2 site preferentially incorporates heavy REE (HREE; Fleet and Pan, 1994, 1995a,b, 1997a; Fleet et al., 2000a,b; Hughes et al., 1991).

The most extensive amount of REE substitution into igneous apatite (up to 27 wt.% REE_2O_3) has been reported from the Ilímaussaq complex in South Greenland (Rønsbo, 1989, 2008). The Ilímaussaq complex is a textbook example for the essentially closed-system evolution of an alkaline plutonic system (e.g., Larsen and Sørensen, 1987; Marks and Markl, in press) and is an economically important REE deposit (e.g., Marks and Markl, in press; Parsons, 2012; Sørensen et al., 2011). It is therefore perfectly suited for the study of the REY-enrichment processes related to magmatic differentiation and hydrothermal REY mobilization and

* Corresponding author at: Universität Tübingen, FB Geowissenschaften, Wilhelmstrasse 56, 72074 Tübingen, Germany.
E-mail address: azirner@uni-bonn.de (A.L.K. Zirner).

http://dx.doi.org/10.1016/j.lithos.2015.04.013
0024-4937/© 2015 Published by Elsevier B.V.

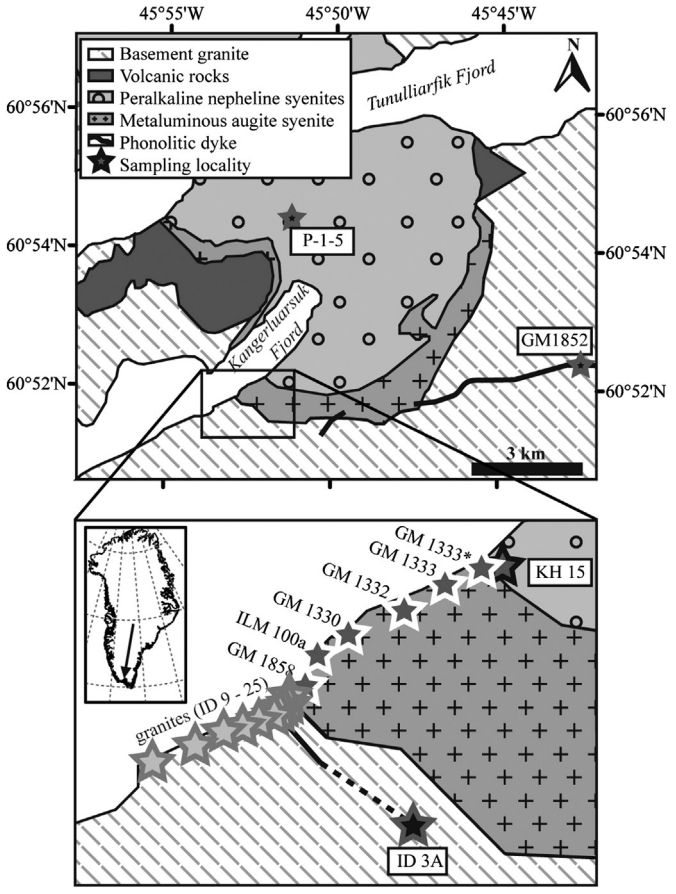


Fig. 1. Simplified geological map of the southern part of the Ilímaussaq intrusion along with sampling localities (modified after Larsen and Steenfelt (1974)). White-rimmed stars correspond to sampling localities of augite syenites, light gray-rimmed to granite samples, dark gray-rimmed to evolved samples and the black-rimmed star corresponds to the augite syenite autolith sample.

redistribution. In the present study we expand the existing data for apatite from the Ilímaussaq complex and its granitic country rocks. Furthermore, we investigate the compositional evolution of apatite during fluid–melt–rock interaction and late-stage metasomatism, and discuss the stability relations between apatite and monazite.

2. Geological setting

The 1.16 Ga old Ilímaussaq complex is a rift-related intrusion of the Gardar Province in South Greenland (e.g., Upton, 2003, 2013) and is an intensively studied alkaline to peralkaline multiphase plutonic complex (e.g.,Marks and Markl, in press; Sørensen, 2001; Sørensen et al., 2006). The Ilímaussaq rocks were emplaced into calc-alkaline granodiorites and granites of the Julianehåb batholith that formed at around 1.8 Ga and represent the core of the Ketilidian orogeny (Allaart, 1976; Chadwick and Garde, 1996; Garde, 2002; Henriksen et al., 2009).

The Ilímaussaq rocks are some of the most extreme products of magmatic differentiation processes known and comprise some of the most unusual magmatic rocks – both in terms of mineralogy and geochemistry (e.g., Bailey et al., 2001; Ferguson, 1964). Furthermore, Ilímaussaq is the type locality of agpaitic rocks, which are a sub-group of peralkaline rocks containing complex Na–Ca–HFSE silicates like eudialyte and aenigmatite instead of otherwise common zircon and/or titanite (Marks et al., 2011; Sørensen, 2001).

To date, it is believed that the Ilímaussaq rocks crystallized from melts that originated from a deep-seated fractionating alkali basaltic magma chamber, from where several successive melt batches were extracted (e.g., Larsen and Sørensen, 1987; Marks et al., 2004a). The first magma batch crystallized to metaluminous augite syenite, followed by peralkaline granites, and the volumetrically dominant third stage, which comprises several varieties of peralkaline mostly agpaitic nepheline syenites. A several tens of meters wide zone of very coarse-grained agpaitic rocks (the so-called border pegmatite) separates the marginal augite syenite shell from the agpaitic nepheline syenites. Detailed petrographic descriptions of the major Ilímaussaq rocks were given by e.g., Ferguson (1964), Hamilton (1964), Sørensen et al. (2006) and Ussing (1912).

Based on fluid-inclusion data (Konnerup-Madsen and Rose-Hansen, 1984) and estimated overburden (Poulsen, 1964), the pressure of emplacement of the Ilímaussaq intrusion was estimated to be about 1 kbar. The evolution of the Ilímaussaq magmas is characterized by a large crystallization interval from >1000 to probably <500 °C, with a strong decrease of silica activity from initially about 0.8 to values as

Table 1
Rock samples containing apatite investigated during this study.

Sample	Distance to contact [m]	Rock type	Facies	Apatite textures	Apatite grain size [mm]
ID 25	−350	Calc-alkaline granodiorite	Not metasomatized	Homogeneous cores	0.02–0.05
ID 21	−170	Calc-alkaline granodiorite		Homogeneous cores	0.02–0.05
ID 19	−115	Calc-alkaline granodiorite	Metasomatically altered	Homogeneous cores	0.02–0.05
ID 17	−55	Calc-alkaline granodiorite		Homogeneous cores	0.02–0.05
ID 16	−25	Calc-alkaline granodiorite		Homogeneous cores	0.02–0.05
ID 14	−8.2	Calc-alkaline granodiorite		Homogeneous cores	0.02–0.05
ID 13	−3.7	Calc-alkaline granodiorite		Homogeneous cores	0.02–0.05
ID 12	−2.5	Calc-alkaline granodiorite		Homogeneous cores	0.02–0.05
ID 11	−1.7	Calc-alkaline granodiorite		Homogeneous cores	0.02–0.05
ID 9	0	Hybrid rock	Mixed and mingled contact	Resorbed overgrowth	0.02–0.5
ILM 100a	30	Augite syenite	Marginal part	Homogeneous cores	
GM 1858	0	Augite syenite	Marginal part	Homogeneous cores, acicular apatite	0.05–0.3 0.02 × 0.5
GM 1330	150	Augite syenite	Middle part	Overgrowth textures, concentric zonation	0.05–0.3
GM 1332	300	Augite syenite	Middle part	Overgrowth- and conversion textures	0.03–0.5
GM 1333	450	Augite syenite	Middle part	Overgrowth textures	0.05–0.3
GM 1333*	600	Augite syenite	Inner part	Overgrowth- and conversion textures, occurrence of monazite	0.05–0.3
KH 15		Augite syenite autolith	Transitional	Overgrowth- and conversion textures (patchy zoning)	0.3 0.01–0.02
GM 1852		Fe-rich peralkaline phonolitic dyke		Oscillatory zoning of cores, overgrowth and conversion	0.01–0.02
P-1-5		Pulaskite		Sector, oscillatory and patchy zoning	0.01–0.7
ID 3A	−30	Agpaitic vein		Oscillatory and patchy zoning	0.15–0.5

low as about 0.3 (Markl et al., 2001). Water activity on the other hand is thought to have strongly increased, as indicated by an early methane-dominated fluid at high temperatures and an almost pure aqueous fluid during later stages (e.g., Krumrei et al., 2007). Relative oxygen fugacity decreased during the augite syenite stage from about f_{O2} = FMQ-1 to below FMQ-4 and rose again to values well above the FMQ buffer during further fractionation and cooling of the agpaitic rocks (e.g., Markl et al., 2001; Marks and Markl, 2001, in press).

3. Sample material

For this study we investigated apatite from several Ilímaussaq rocks and the surrounding granitic country rocks (Fig. 1; Table 1) in order to explore the effects of (i) magmatic differentiation, (ii) metasomatic overprint and (iii) contact metamorphism on apatite composition and stability. Many of the samples have been subject to earlier petrological and geochemical studies (e.g., Markl et al., 2001; Marks and Markl, 2001, in press; Marks et al., 2004b, 2007).

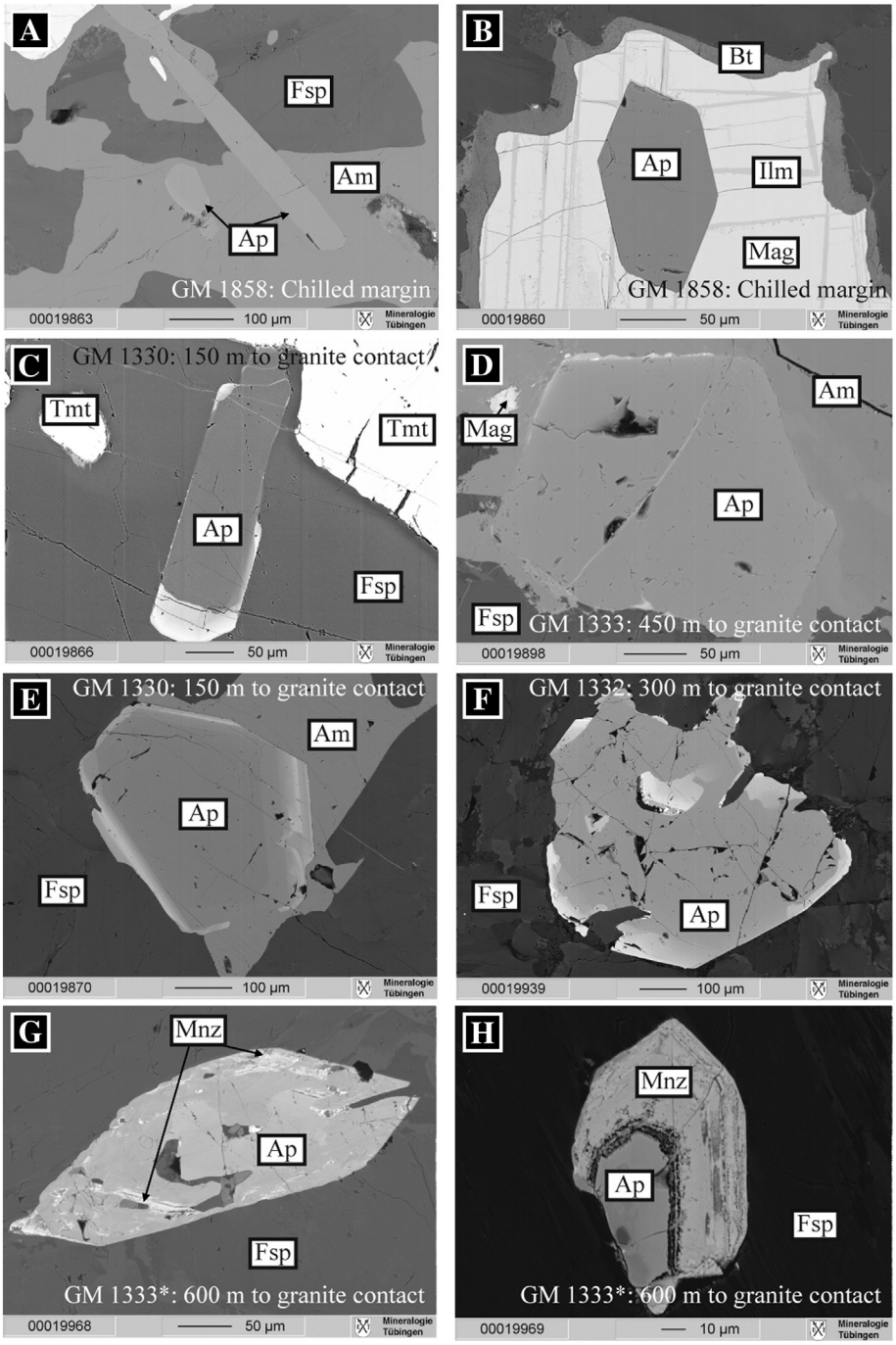


Fig. 2. Apatite textures within augite syenites (BSE images). A) Acicular apatite needle as an inclusion in feldspar and amphibole. B) Euhedral apatite inclusion in titano magnetite (displaying exsolution lamellae of ilmenite) being rimmed by biotite. C) Apatite inclusion in alkali feldspar. The dark gray inner part of the crystal is interpreted as representing the primary magmatic composition, which was later resorbed and overgrown by REY-enriched apatite. D) Fractured apatite as inclusion in amphibole, overgrown by a narrow seam of REY-enriched apatite. E) Concentric zoned apatite inclusion in feldspar and amphibole. F) Subhedral fractured and porous apatite inclusion in feldspar displaying REY-enriched overgrowth textures and conversion textures. G) and H) Apatite–monazite textures from augite syenite sample (GM 1333*) with G) apatite as inclusion in feldspar displaying monazite inclusions and growth along cracks and H) apatite being overgrown by monazite while retaining the crystal shape of the apatite.

Samples from the augite syenite unit represent a traverse parallel to the assumed direction of crystallization (Fig. 1; Table 1). They consist of perthitic alkali feldspar, fayalitic olivine, Ca-rich augite, Fe–Ti oxides, and calcic amphibole, with minor amounts of nepheline, biotite, apatite, zircon/baddeleyite, and various sulfides.

One sample from the border pegmatite (KH 15) was investigated during this study (Fig. 1; Table 1). It mainly consists of a very coarse-grained agpaitic mineral assemblage (alkali feldspar, sodic amphibole and pyroxene, aenigmatite, nepheline and eudialyte), which overgrows aggregates of augite, Fe–Ti oxides, and apatite that are most likely relics of an augite syenite autolith. One pulaskite sample was chosen for this study (Fig. 1; Table 1). This coarse-grained rock consists of cumulus alkali feldspar, olivine, augite, Fe–Ti oxides, and apatite, with intercumulus sodic amphibole and pyroxene, aenigmatite, biotite, nepheline, analcime, and fluorite, partly replacing early olivine, augite, and Fe–Ti oxides. In many of the nepheline syenites, apatite is rare or absent. Therefore, one about 15 cm wide apatite-bearing agpaitic vein (ID 3A) was studied that transects the granitic country rocks (Fig. 1; Table 1). The vein further contains sodic amphibole and pyroxene, eudialyte, alkali feldspar quartz, and albite. Also, one sample from a spatially associated agpaitic peralkaline Fe-rich phonolitic dyke rock (GM 1852) was investigated that may represent a small-scale equivalent of the Ilímaussaq complex (e.g., Larsen and Steenfelt, 1974; Marks and Markl, 2003) (Fig. 1; Table 1). This sample contains a phenocryst assemblage equivalent to the augite syenite stage (olivine, augite, Fe–Ti oxides, alkali feldspar, and apatite) and an agpaitic groundmass assemblage (albite, microcline, nepheline, sodalite, sodic amphibole, sodic pyroxene, aenigmatite, eudialyte, astrophyllite, hjordahlite, and fluorite).

Several samples from the granitic country rocks (ID 9–25) collected at various distances from the contact towards the augite syenite unit (Fig. 1; Table 1) were also investigated. Sample ID 9 is a hybrid rock between augite syenite and granite. It originates from the approximately 2 m wide contact zone, which is marked by intensive mixing and mingling of augite syenite with pockets of granite that seems to have back-veined into the augite syenite (Ferguson, 1964). Unlike the other samples in this group, it contains neither biotite nor plagioclase but is rich in alkali feldspar and quartz. Amphibole is the only mafic mineral and accessory minerals are zircon, ilmenite and apatite. Sample IDs 10–25 show typical granitic mineral assemblages

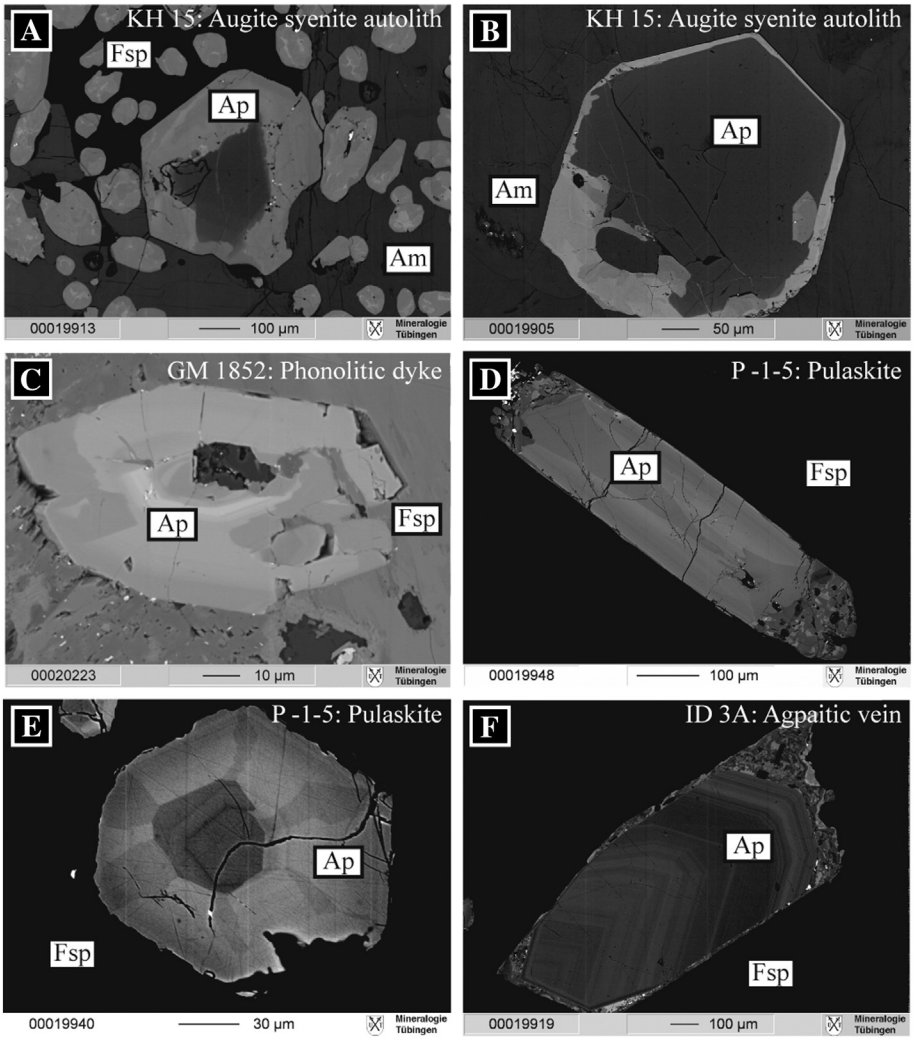


Fig. 3. Apatite textures from evolved rocks. A) and B) Apatite inclusions in amphibole from the augite syenite autolith (KH 15). Small crystals are patchily zoned. Larger crystals exhibit a dark gray core, which is resorbed and overgrown by a REY-enriched, patchily zoned rim. In some cases, euhedral apatites occur along the interface between the core and resorption rims. C) Apatite, which shows oscillatory zoning in the core and displays conversion textures towards the rim. These apatites are from within an associated phonolitic dyke rock (GM 1852). D) Sector-zoned apatite from a pulaskite (P-1-5), which is resorbed and overgrown by patchily zoned apatite on both sides. E) Sector zoned apatite inclusion in feldspar from the same sample (P-1-5) displaying an oscillatory zoned core. F) Oscillatory zoned apatite from an agpaitic vein (ID 3A), resorbed and overgrown by a patchy seam.

(quartz, plagioclase, alkali feldspar, biotite with minor amounts of Fe–Ti oxides, apatite, titanite, and zircon) some of them with minor amounts of various types of pyroxenes and amphiboles that are believed to have been formed due to the intrusion of the Ilímaussaq melts (for details see Marks and Markl (in press)).

4. Analytical methods

Major and minor elements in apatite were determined by electron probe microanalysis (EPMA) at the Fachbereich Geowissenschaften, Universität Tübingen, Germany using a JEOL JXA8900 RL electron microprobe operated in wavelength dispersive mode (WDS). The probe current was set to 10 nA and acceleration voltage to 15 kV. Apatite grains were analyzed with a defocused beam (10 μm) to avoid Na, F, and Cl migration (Stormer, 1993). Natural and synthetic standards were used for calibration with the Durango apatite crystal as a calibration standard for Ca, P, and F, similar to Marks et al. (2012) and Wang et al. (2014). Data reduction was performed using the internal ZAF matrix correction of JEOL (Armstrong, 1991).

Trace elements were analyzed at the Institut für Geowissenschaften, Universität Mainz, Germany using an Agilent 7500ce quadrupole ICP-MS coupled to a New Wave Research UP 213 laser ablation system with a frequency quintupled Nd:YAG laser (213 nm wavelength, Jacob, 2006). Dwell times for each isotope were 10 ms and the spot sizes during the analyses were 20–75 μm. Ablation of most apatites resulted in round and regular ablation pits. In small apatite grains, however, catastrophic ablation was frequently observed. A mixture of He and Ar was used as the carrier gas. The ablation was carried out with an energy density of 4 J/cm^2 and a pulse rate of 5 Hz. The commercial software GLITTER 4.0 (Macquarie University) was used for data reduction with NIST SRM 612 as the external standard and ^{43}Ca as the internal standard using Ca concentrations obtained by EPMA. Data for NIST SRM 612 were taken from the GeoReM database (Jochum and Nohl, 2008).

5. Results

5.1. Apatite textures

Apatite is euhedral to subhedral in all the investigated samples, in cases fractured and etched. It occurs as inclusions in most other mineral phases or along grain boundaries between them (Figs. 2–4). It is columnar in most samples and shows variable grain-sizes, with relatively coarse-grained apatite (up to 0.7 mm large) occurring in augite syenites and some of the evolved rocks and relatively fine-grained apatite (<100 μm large) being typical for granitic country rock samples (Fig. 4A and B; Table 1). In a marginal augite syenite sample (GM 1858), additional acicular apatite is present with diameters mostly less than 20 μm but up to 0.5 mm in length (Fig. 2A; Table 1).

Based on BSE imaging, apatite crystals with homogeneous core regions (denoted as core compositions) occur in all augite syenites (Fig. 2; Table 1). In several samples, however, some apatite grains are overgrown by relatively bright regions (denoted as overgrowths), having compositions with higher average atomic numbers, in these cases mostly due to REY enrichment (see later). In cases, these bright REY-enriched rims seem to resorb the primary magmatic core (Fig. 2C and D) and rarely a bright-appearing REY-enriched (and younger) apatite generation develops in the interior of the larger apatite grains (denoted as conversion textures; Fig. 2F; Table 1). Few apatites display a concentric zonation with several ca. 5–10 μm wide growth zones (Fig. 2E; Table 1). The innermost augite syenite sample (GM 1333*) contains additional monazite that overgrows precursor apatite (Fig. 2G) and contains monazite as inclusions and along cracks in apatite (Fig. 2H).

In the augite syenite autolith (KH 15) homogeneous cores of coarse apatite grains are partly resorbed and overgrown by patchy and irregularly zoned apatite (Fig. 3A; Table 1). The interface between cores and irregularly zoned rims may be sharp or diffuse and in some cases, REY-enriched and euhedral apatite inclusions (denoted as conversion textures) are present along the interface between the core and rim (Fig. 3B; Table 1). Closely associated fine-grained apatites invariably

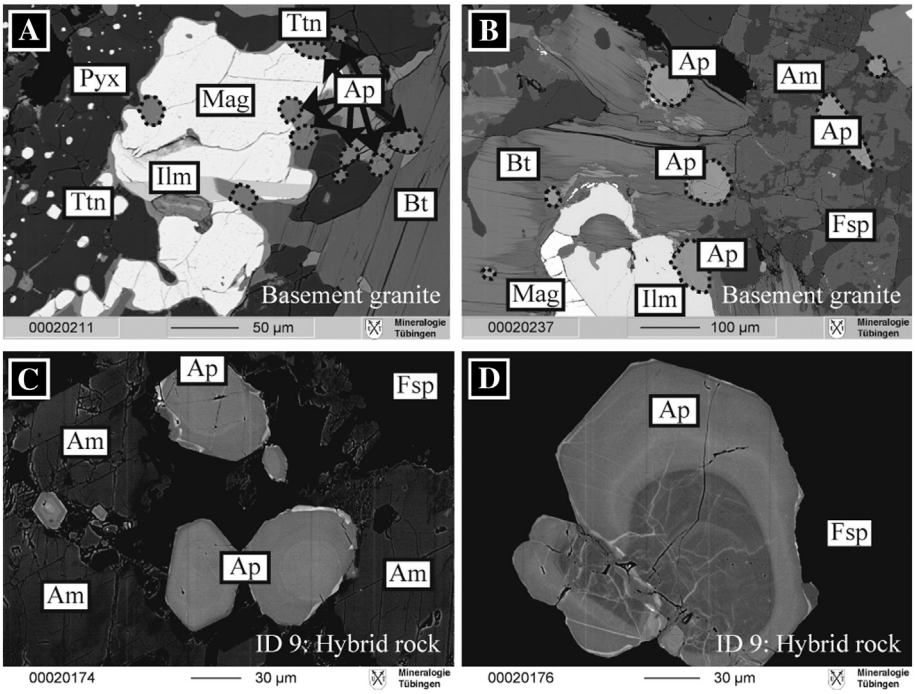


Fig. 4. Apatite textures (BSE images) within the basement granite samples. (A) and (B) (show homogeneous crystals) apatites as typically present in the granites. (C) and (D) illustrate apatite textures from the hybrid rock at the contact zone between the augite syenite and granitic country rocks. Note the rounded apatite cores.

show patchy zonation (Fig. 3A). In the phonolitic dyke rock, similar zoning textures as in augite syenites and the augite syenite autolith occur (Fig. 3C; Table 1).

In the pulaskite (P-1-5), most apatites are sector-zoned (Fig. 3D and E; Table 1), whereas in the agpaitic vein (ID 3A), oscillatory zoning is common (Fig. 3F; Table 1). In both samples, however, some apatite grains are overgrown by patchy and irregularly zoned apatite (Fig. 3D and F; Table 1).

In most granite samples (ID 11–25), apatite does not show any obvious zoning textures (Fig. 4A and B; Table 1). Apatite from the hybrid rock (ID 9), however, displays zoning textures with REY-poor, rounded cores and younger overgrowth (Fig. 4C and D; Table 1).

5.2. Compositional variability

Major- minor- and trace element data for the various apatite types are given in the electronic appendix. Apatite in all samples is F-dominated (≥80 mol% apatite-(F)) with very low amounts of Cl (≤0.1 wt.%) and minor amounts of calculated OH, which is typical of most plutonic rocks (Piccoli and Candela, 2002). However, large compositional differences are present with regards to their Na, Si and REY contents.

During EPMA analyses, La and Ce were analyzed as proxies for the total REE content of apatites. Many of the studied apatites contain <3 wt.% $La_2O_3 + Ce_2O_3$ (Fig. 5). In such analyses, the heavier LREE (Pr, Nd, Sm), the MREE and the HREE would be close to or below the detection limit of EPMA which would render most of these values meaningless. Therefore, we did not include heavier LREE, MREE and HREE in our EPMA protocol. Some apatites of the evolved rocks are very REE-rich, and the EPMA totals for such apatites imply up to about 5 wt.% of missing REE. However, because of the high masses of REE, the effects on the formula calculation are relatively minor. Nevertheless, additional REE data were obtained by LA-ICP-MS (Fig. 6) and the comparison with EPMA data (Fig. 7) shows that the omission of heavier REE's during EPMA has no significant effect on our derived conclusions.

Apatites from all augite syenites, the augite syenite autolith and the phonolitic dyke rock have similar core compositions (~0.8 wt.% $La_2O_3 + Ce_2O_3$, ~0.3 wt.% SiO_2, and ~0.05 to 0.2 wt.% Na_2O) (Fig. 5). The various zonation and overgrowth textures, however, reveal much higher $La_2O_3 + Ce_2O_3$ (up to 14 wt.%) and SiO_2 (up to 9 wt.%) contents. Similarly, these textures are enriched in Na_2O (up to 1.0 wt.%), except for augite syenites, where the various overgrowth textures contain similar amounts of Na_2O as the homogeneous core regions (Fig. 5). Chondrite-normalized REY patterns from apatite in augite syenites show LREE-enrichment and a prominent negative Eu-anomaly (Eu/Eu*

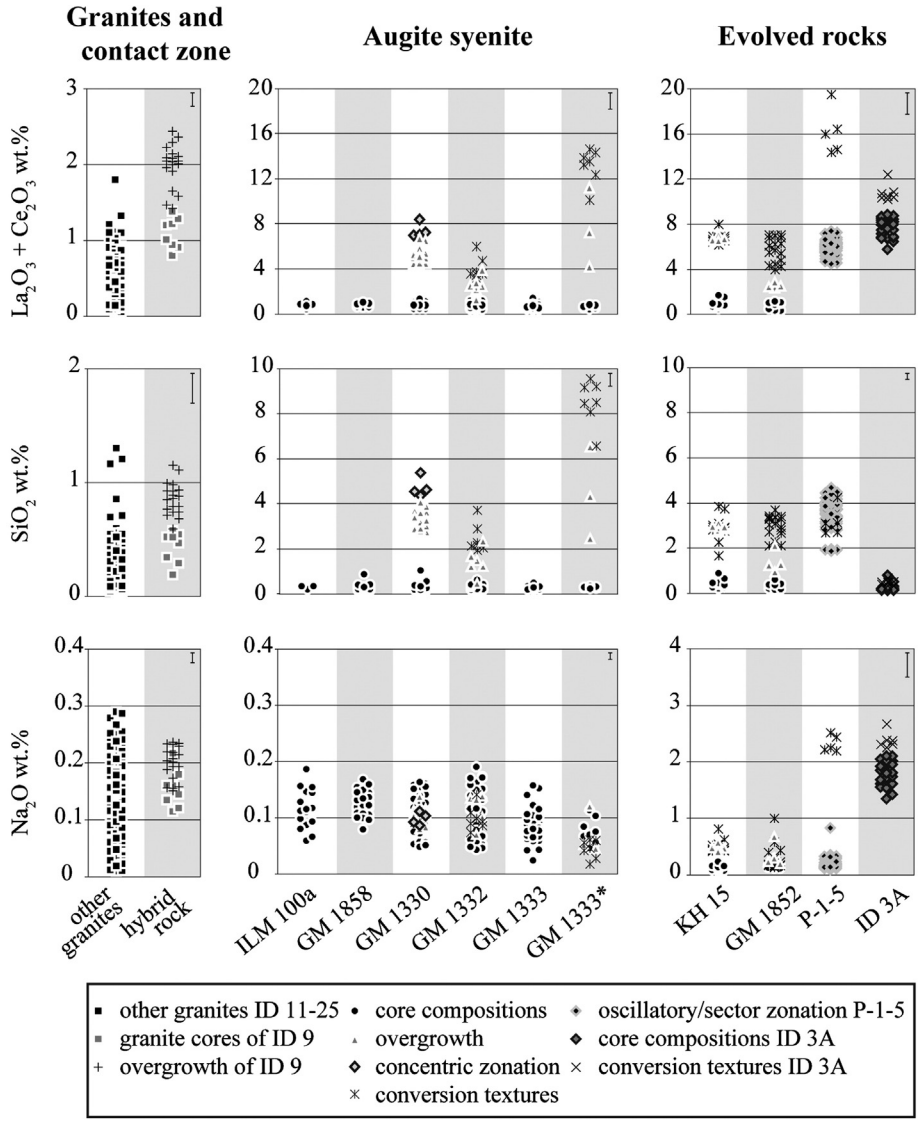


Fig. 5. Variations in the $La_2O_3 + Ce_2O_3$, SiO_2, and Na_2O contents in the various apatite textures from the investigated samples.

~0.25) for the apatite cores (Fig. 6A) and are shifted towards higher concentrations for the overgrowth and zonation texture, with even stronger negative Eu-anomalies (Eu/Eu* ~0.15) and slightly negative Y-anomalies. In the augite syenite autolith (KH 15) and the phonolitic dyke (GM 1852), the apatite core REY patterns are similar to those from the zoned part of the apatites from the augite syenite (Fig. 6A). Overgrowth textures for KH 15, however, are higher in LREE but similar in HREE compared to the core compositions and the patterns are therefore much steeper (Fig. 6A).

Sector-zoned apatite from the pulaskite (P-1-5) contains up to 8 wt.% $La_2O_3 + Ce_2O_3$, 5 wt.% SiO_2, similar to the rims of apatite from the augite syenite autolith (KH 15) and the phonolitic dyke (GM 1852) (Fig. 5). Their Na_2O contents (about 0.25 wt.%) are slightly higher. Apatite from overgrowth textures in this sample are very rich in $La_2O_3 + Ce_2O_3$ (up to 20 wt.%) with similar SiO_2 contents but much higher Na_2O (2.5 wt.%) compared to sector-zoned apatites (Fig. 5). Compared to the REY patterns from the augite syenite, LREE are extremely enriched, and the negative anomalies for Eu (Eu/Eu* ~0.29) and Y are even more pronounced (Fig. 6B).

Oscillatory zoned cores of apatite from the agpaitic vein (ID 3A) display similar $La_2O_3 + Ce_2O_3$, contents (up to 8.5 wt.%) as those from the pulaskite, apatite rims from the augite syenite autolith and the phonolitic dyke. They are however, much lower in SiO_2 (<1 wt.%) and much higher in Na_2O (up to 2.7 wt.%) than any of the other samples (Fig. 5). Also, they have high concentrations of Sr but are comparatively low in U, Th, and Zr, which might be related to the presence of eudialyte in this sample. Their REY patterns are very steep. HREE from the irregular overgrowths are higher than in cores, whereas the LREE are slightly lower (Fig. 6B).

Apatite from granites (ID 11–25) do not show any systematic compositional variation and contain up to 1.9 wt.% $La_2O_3 + Ce_2O_3$, 3.5 wt.% SiO_2, and 0.3 wt.% Na_2O (Fig. 5). Apatites from the hybrid rock (ID 9), however, display clear compositional differences between the resorbed cores and overgrowths: The latter are enriched in $La_2O_3 + Ce_2O_3$ (up to 2.5 wt.%), SiO_2 (up to 1.2 wt.%), and Na_2O (up to 0.25 wt.%), compared to the core compositions (Fig. 5). In contrast to the REY patterns from the other granitic samples, both the resorption rims and the core compositions of apatite from ID 9 display pronounced

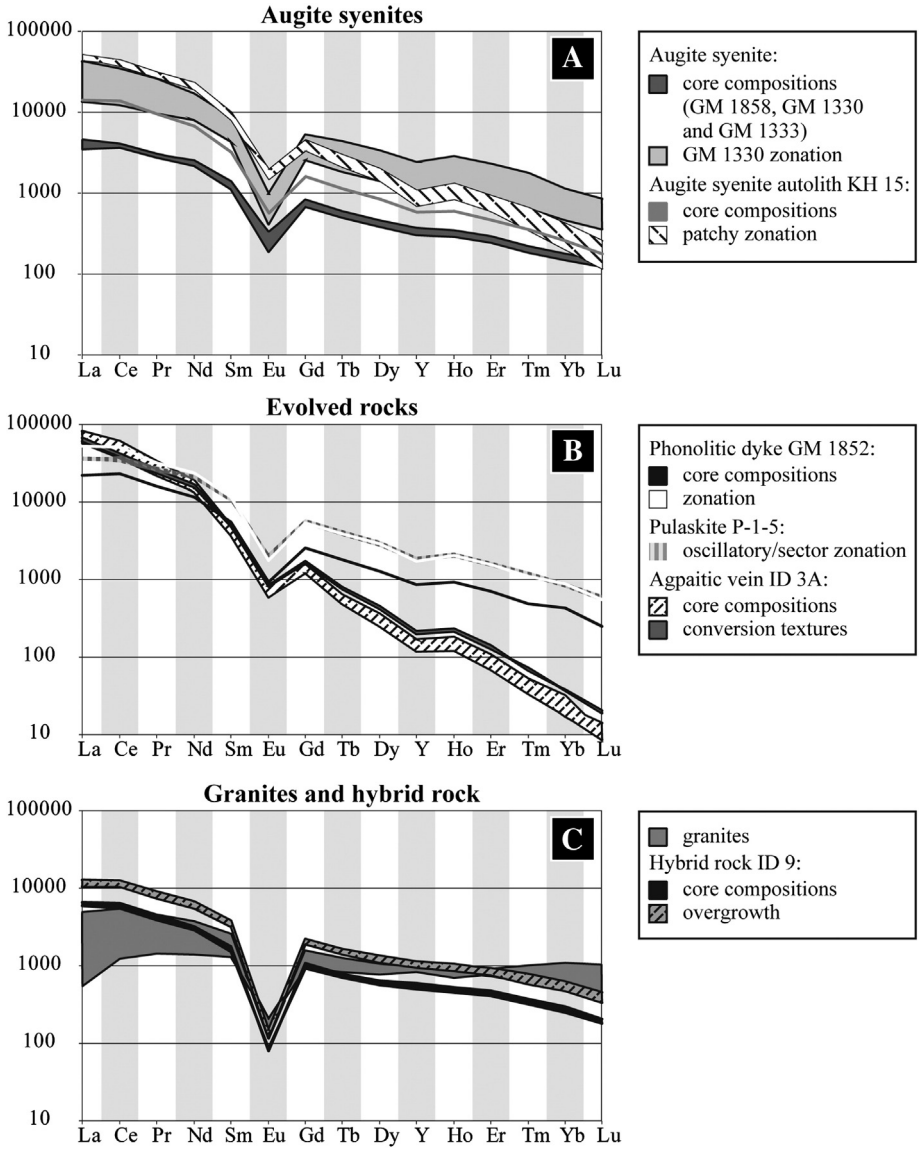


Fig. 6. Chondrite-normalized REY patterns for apatite from various samples and zonation types. A) Augite syenites, B) evolved rocks and C) granitic host rocks. (Note that Pm is not included so it is not a true atomic number plot and rather represents typical REE patterns.)

negative Eu-anomalies (Eu/Eu* ~0.06). Also, the REY of the overgrowth zones are shifted to slightly higher concentrations (Fig. 6C).

6. Discussion

The various zoning textures combined with compositional data will be presented here in order to discuss the influence of magma differentiation and metasomatic processes on apatite textures, composition, and stability and to explore structural aspects of REY-uptake in more detail.

6.1. Interpretation of various apatite textures and zoning patterns

Acicular apatite crystals, similar to those found in the fine-grained marginal sample from the augite syenite, (Fig. 2A) commonly grow during very fast crystallization and cooling (e.g., Wyllie et al., 1962) and/or the presence of a fluid (Capdevila, 1967). Such apatite crystals may represent a very early apatite generation, but cannot be reliably analyzed by EPMA because of their small size.

Homogeneous apatite cores from the augite syenites (Fig. 2) crystallized from an early melt composition. As these apatites display very similar core compositions in all the augite syenite samples (Figs. 5 and 6A), we argue that the melt composition from which the apatite crystallized was very similar for all samples, despite their variable degree of differentiation, as indicated by X_{Mg} values from the mafic minerals and the increasing modal abundance of nepheline (Marks and Markl, 2001). Concentrically-zoned apatite rims (e.g. in sample GM 1330; Fig. 2E) probably crystallized from evolved interstitial melts and indicate apatite growth during a rather long crystallization interval.

Oscillatory zonation in apatite is especially common in the evolved rocks of Ilímaussaq (P-1-5, GM 1852 and ID 3A; Fig. 3F). It is a primary non-equilibrium growth texture, particularly occurring in magmatic (notably in alkaline rocks) and is well-known from many rock-forming minerals (Shore and Fowler, 1996), including apatite (e.g., Kempe and Götze, 2002; Rakovan and Reeder, 1996; Rønsbo, 1989). The composition of alternating REY-enriched vs. Ca + P-enriched layers is controlled by the relative diffusion of the elements in the melt as opposed to the crystal, i.e. when a REE-enriched layer forms, the local melt is depleted in REE allowing for a REE-depleted layer to form. By the time, diffusion of REY in the melt near the new layer has been brought up to the original concentration, the next layer to be REY-enriched forms.

Sector zonation as found in apatite from sample P-1-5 (Fig. 3D and E) is characterized by different compositions in different growth sectors of a single crystal (Dowty, 1976). Compositional differences among the growth sectors are not produced by disequilibrium crystallization but form because of different local equilibria between the various growth surfaces and their identical host environment (van Hinsberg and Schumacher, 2007). Sector-zoned pyroxene and eudialyte are known from the agpaitic nepheline syenites (sodalite foyaite and naujaite which also belong to the Ilímaussaq roof sequence as pulaskite) from Ilímaussaq and elsewhere (e.g., Schilling et al., 2011; Shearer and Larsen, 1994). For pyroxene, Shearer and Larsen (1994) showed that the REY are accommodated in the M2 site by the two coupled substitutions $2Ca^{2+} \leftrightarrow Na^{+} + REE^{3+}$ and $Ca^{2+} + Si^{4+} \leftrightarrow REE^{3+} + Al^{3+}$ and that the uptake of LREE and MREE is dependent on the M2 site, which may apply for apatite as well (see below).

The various overgrowth and conversion textures are probably related to late magmatic to hydrothermal processes, and formed during the metasomatic overprint with REY-enriched melts and/or fluids. Rae et al. (1996) proposed that high REE concentrations in apatites from syenites in the North Qôroq center, another intrusion of the Gardar Province, were originally caused by magmatic processes, while the apatite zonation textures were probably related to successive pulses of metasomatic fluids. For example, the homogeneous cores of apatites from the augite syenite autolith (KH 15) (Figs. 3A) most likely represent inherited apatites from the augite syenite stage. These cores are partly resorbed and overgrown by patchy apatite enriched in Na, Si, REY, and several trace elements such as Sr, U, Th, Pb, Mn, Ti, and Zr (Figs. 3A, B, 5 and 6A). These patchy rims probably formed due to interaction with a peralkaline melt/fluid derived from the evolved agpaitic rocks of the Ilímaussaq complex. The texturally and compositionally very similar small apatites from the same sample (Figs. 3A and 6) either represent completely overprinted apatite or grains that nucleated and grew during metasomatism. Similar resorption textures were found in one granite sample from the contact zone towards the augite syenite (Fig. 4C and D) and imply infiltration of REY out of the Ilímaussaq complex into the granitic host rocks.

We conclude that primary magmatic apatite compositions are preserved in all of the studied samples. They are preserved as homogeneous cores or as oscillatory- or sector-zoned grains. In several samples, various types of overgrowth and conversion textures indicate the late-stage interaction with REY-enriched melts and/or fluids.

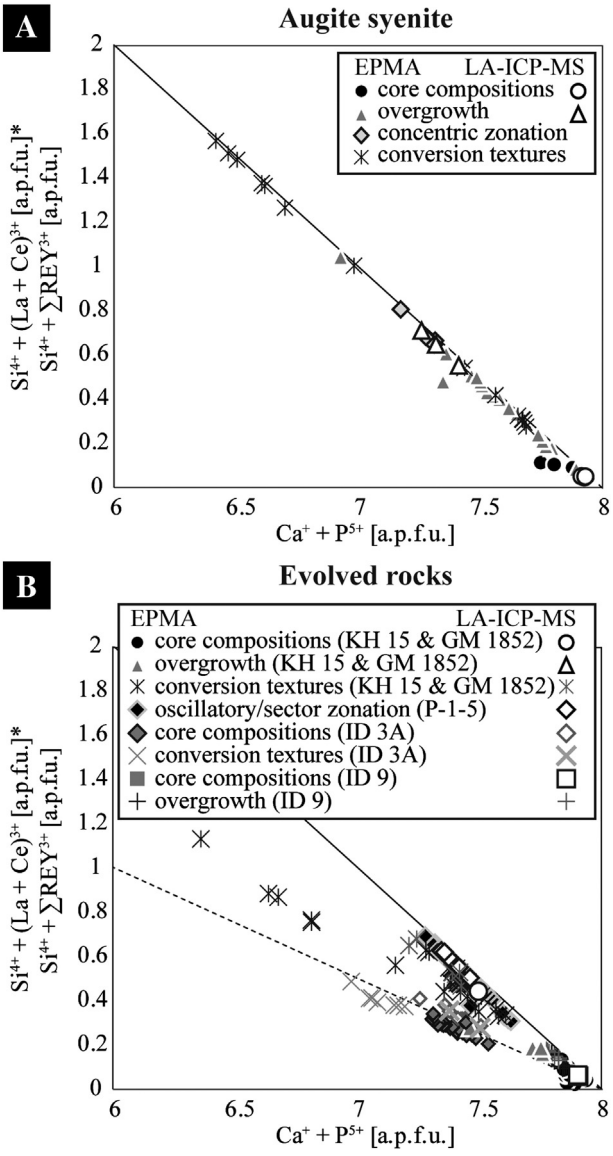


Fig. 7. Variations in Ca, Na, REY, Si, and P for apatite shown in substitution diagrams from A) augite syenites and B) evolved rocks. * refers to EPMA analyses.

6.2. Substitution mechanisms involving REY incorporation

Compositional data on apatite from various Ilímaussaq rocks have previously been reported (Rønsbo, 1989, 2008), revealing their compositional diversity and complexity in terms of REE incorporation. For REE-uptake in apatite, several charge-compensating coupled substitution mechanisms have been proposed (Pan and Fleet, 2002 and references therein). As shown by Rønsbo (1989, 2008), the two most important ones for the Ilímaussaq rocks are

$$Ca^{2+} + P^{5+} \leftrightarrow Si^{4+} + REY^{3+} \quad (1)$$

$$2\,Ca^{2+} \leftrightarrow Na^{+} + REY^{3+}. \quad (2)$$

Chemical compositions of apatite from the augite syenite follow largely coupled substitution (1) and the most Si and REY-rich analyses approach ~30 mol% of the britholite end member (Fig. 7A). This is consistent with earlier data (Rønsbo, 1989, 2008) but was explained as an approach to a lessingite end member composition [$Ca_2REE_3(SiO_4)_3(OH,F,Cl)$]. However, according to the new nomenclature of the apatite supergroup, it should be rather called britholite-Ce (Pasero et al., 2010).

In contrast, and consistent with earlier findings of Rønsbo (1989, 2008), coupled substitution (2) becomes increasingly important in apatite from agpaitic samples and from samples, which might be influenced by agpaitic melts/fluids (Fig. 7B). For example, the core compositions of apatites from the augite syenite autolith largely resemble augite syenite compositions, but their REY-rich overgrowths show variable contributions from coupled substitution (2). Similarly, REY incorporation in oscillatory-zoned apatite cores from the phonolitic dyke rock (Fig. 3C), which crystallized from an agpaitic melt, follows partly coupled substitution (2). Apatites from the pulaskite sample (P-1-5) exhibit the highest Si and relatively lowest Na contents (Fig. 5). Incorporation of REY in these apatites mostly follows coupled substitution (1) but for REY-rich compositions, coupled substitution (2) becomes more important (Fig. 7B). Apatites from the agpaitic vein (ID 3A) exhibit the highest Na contents (Fig. 5). They have similar REY-contents compared to apatite rims found in some of the augite syenite samples but are very low in Si (Figs. 5 and 6B). The REY are largely incorporated following coupled substitution (2) (Fig. 7B). The fact that equally REY-rich apatite compositions from the augite syenite and the highly evolved agpaitic vein (Figs. 5, 6 and 7) were produced by different coupled substitution mechanisms demonstrates that REY-concentrations in apatite do not only depend on the REY concentration of the environment from which the apatite crystallizes, but are also influenced by the relative Na and Si activities in the melt.

In comparing the REY patterns of apatite from the various samples, it is apparent that the decreasing influence of substitution (1) is accompanied by an increasing steepness of the normalized REY plots, expressed in the increasing $(La/Gd)_N$ and $(Gd/Yb)_N$ ratios. Data from natural apatites and experimental work imply that REY uptake in apatite is the highest in the range Nd–Gd and the lowest for Lu and that LREE in apatite primarily substitute on the Ca1 site whereas HREE prefer the Ca2 site (Fleet and Pan, 1995a,b, 1997a,b; Fleet et al., 2000a,b; Hughes et al., 1991). For REE-rich apatite compositions approaching the britholite end member composition, two major cation arrangements exist: $(REE,Ca)_2(REE,Ca)_3[(Si,P)O_4]_3(OH,F)$ and $(Ca,REE)_2(REE,Ca)_3[(Si,P)O_4]_3(OH,F)$. Their main difference is cation ordering on the Ca1 site resulting from differences in the REE-O-bonds (Noe et al., 1993). Possibly, the variable behavior of LREE and HREE between coupled substitutions (1) and (2) indicates that the more common REY substitution for Ca2 favors Eq. (1). The stronger enrichment in LREE observed for apatites from the agpaitic rocks would thus be a result of REY-uptake following Eq. (2) with LREE largely favoring the Ca1 site.

6.3. Formation of monazite versus REE-rich apatite

Previous studies of natural assemblages (e.g., Hansen and Harlov, 2007) as well as experimental investigations (e.g., Harlov et al., 2005) imply that monazite associated with fluorapatite is a potential tracer of metasomatic processes. In our study, the most evolved augite syenite sample (GM 1333*) contains monazite that in some cases overgrows precursor apatite (Fig. 2G), whereas in others, monazite occurs along cracks in apatite (Fig. 2H). Hence, we consider a magmatic origin for the monazite as unlikely and the formation of monazite at the expense of apatite is probably a result of fluid-induced alteration of apatite via coupled dissolution–reprecipitation processes (Harlov and Förster, 2003; Harlov et al., 2005). In such a case, the available REY and P of the apatite provides the material necessary for the nucleation and growth of the monazite (Harlov, 2011).

The stability relations between monazite and fluorapatite crucially depend on fluid composition rather than on prevailing P–T conditions (Budzyń et al., 2011). Whether apatite breaks down to form monazite (Fig. 8 path I) or remains stable (Fig. 8 path II) may be influenced by

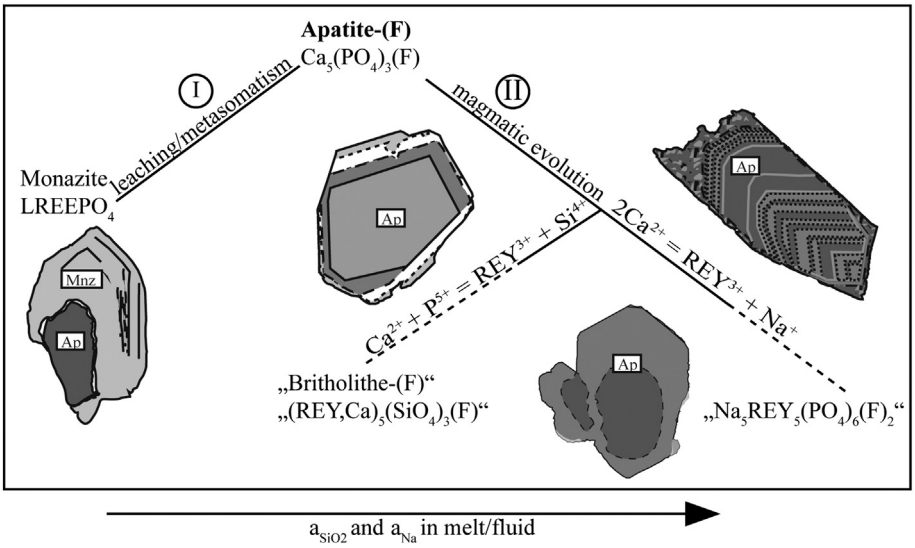


Fig. 8. Different REY-involving incorporation/redistribution mechanisms observed for some Ilímaussaq samples. Path I: Monazite is considered in this case to form due to fluid induced processes and not magmatically. Path II: REY enriched apatite textures are considered to form due to the magmatic evolution of the melt. If apatite ether remains stable to form REY enriched textures or breaks down to form monazite is a function of the melt/fluid composition.

the availability of Na^{+} and Si^{4+} ions to maintain charge balance in the apatite structure. Removal of Na and Si at high REE levels from the system results in charge imbalance freeing the REY to react with P and to form monazite (and/or xenotime). Removal of Si and/or Na without the coupled removal of the REY can occur in Na- and Si-absent fluids such as pure H_2O, H_2O/CO_2, acids such as HCl or H_2SO_4, or a KCl-rich brine (Harlov and Förster, 2003; Harlov et al., 2005). A certain amount of microporosity in apatite is necessary to serve as nucleation sites for monazite inclusion, which may then form according to the simplified chemical reaction:

REY-rich fluorapatite + fluid = monazite + REY-poor fluorapatite.

Accordingly, the formation of monazite in the most evolved augite syenite sample can be explained by reaction of magmatic apatite with a Na- and/or Si-poor aqueous fluid (Fig. 8 path I). It remains, however, unclear why this phenomenon only occurs in the most evolved sample of the investigated augite syenites. Maybe, it is related to the increased abundance of cracks observed in this sample, which was shown to enhance monazite formation (e.g., Harlov et al., 2005).

7. Summary

Apatite textures and compositions from the Ilímaussaq complex (South Greenland) are a powerful tool in deciphering their magmatic history as well as metasomatic processes taking place over a large temperature and time interval. During magmatic differentiation, apatite incorporates successively more REY. In the least evolved rocks of the complex (augite syenites), REY incorporation in apatite follows mainly the coupled substitution mechanism $Ca^{2+} + P^{5+} \leftrightarrow Si^{4+} + REY^{3+}$ (1). With increasing differentiation, however, the substitution $Ca^{2+} \leftrightarrow Na^{+} + REY^{3+}$ (2) becomes more important such that it is the principal REY incorporating coupled substitution mechanism in the more evolved peralkaline rocks of the complex. Both coupled substitution mechanisms can incorporate similar amounts of REY into the apatite. Hence, not only the absolute REY concentration in the melts influence the REY concentration in apatite, but also the availability of other cations, such as Na and Si, involved in the two dominant coupled substitutions.

In many of the investigated samples, magmatic apatite shows variable overgrowth, replacement and zonation textures, invariably enriched in REY and several other trace elements. These are most likely related to late magmatic to hydrothermal processes that formed during the metasomatic overprint with highly evolved melts and/or fluids. Very rarely, monazite was found to replace precursor apatite. Based on textural observations, we suggest that the formation of monazite at the expense of apatite is probably a result of fluid-induced alteration of apatite via coupled dissolution–reprecipitation processes.

Acknowledgments

Special thanks to Insa T. Derrey and Kai Hettmann for sharing their sample material and helpful discussions, to Indra Gill-Kopp for the thin section preparation and to Lisa C. Baldwin and Prof. Peter Belton for the constructive criticism on an earlier version of this manuscript. We highly appreciate the comments of two anonymous reviewers and the editorial handling of Nelson Eby.

Appendix A. Supplementary data

Supplementary data to this article can be found online at http://dx.doi.org/10.1016/j.lithos.2015.04.013.

References

Allaart, J., 1976. Ketilidian mobile belt in South Greenland. In: Escher, A., Watt, W.S. (Eds.), Geology of Greenland. Geological Survey of Denmark, Copenhagen, pp. 120–151.
Armstrong, J.T., 1991. Quantitative Elemental Analysis of Individual Microparticles with Electron Beam Instruments. Plenum Press, pp. 261–315 Electron Probe Quantitation (USA).
Bailey, J.C., Gwozdz, R., Rose-Hansen, J., Sørensen, H., 2001. Geochemical overview of the Ilímaussaq alkaline complex, South Greenland. Geology of Greenland Survey Bulletin 190, 35–53.
Budzyń, B., Harlov, D.E., Williams, M.L., Jercinovic, M.J., 2011. Experimental determination of stability relations between monazite, fluorapatite, allanite, and REE-epidote as a function of pressure, temperature, and fluid composition. American Mineralogist 96 (10), 1547–1567.
Capdevila, R., 1967. Extension du metamorphisme regional hercynien dans le Nord-Ouest de l'Espagne (Galice orientale, Asturies, Leon). Société Géologique de France 7, 277–279.
Chadwick, B., Garde, A.A., 1996. Palaeoproterozoic oblique plate convergence in South Greenland: a reappraisal of the Ketilidian Orogen. Geological Society, London, Special Publications 112 (1), 179–196.
Dowty, E., 1976. Crystal structure and crystal growth: II. Sector zoning in minerals. American Mineralogist 61 (5-6), 460–469.
Elliott, J.C., Wilson, R.M., Dowker, S.E.P., 2002. Apatite structures. Advances in X-Ray Analysis 45, 172–181.
Ferguson, J., 1964. Geology of the Ilímaussaq alkaline intrusion, South Greenland: Description of map and structure. Meddelelser om Grønland, Copenhagen.
Fleet, M.E., Pan, Y., 1994. Site Preference of Nd in Fluorapatite [Ca10(PO4)6F2]. Journal of Solid State Chemistry 112 (1), 78–81.
Fleet, M.E., Pan, Y., 1995a. Site preference of rare earth elements in fluorapatite. American Mineralogist 80 (3), 329–335.
Fleet, M.E., Pan, Y., 1995b. Crystal chemistry of rare earth elements in fluorapatite and some calc-silicate minerals. European Journal of Mineralogy 7 (3), 591–605.
Fleet, M.E., Pan, Y., 1997a. Site preference of rare earth elements in fluorapatite: Binary (LREE + HREE)-substituted crystals. American Mineralogist 82 (9), 870–877.
Fleet, M.E., Pan, Y., 1997b. Rare earth elements in apatite: Uptake from H_2O-bearing phosphate–fluoride melts and the role of volatile components. Geochimica et Cosmochimica Acta 61 (22), 4745–4760.
Fleet, M.E., Liu, X., Pan, Y., 2000a. Rare-earth elements in chlorapatite [Ca10(PO4)6Cl2]: Uptake, site preference, and degradation of monoclinic structure. American Mineralogist 85 (10), 1437–1446.
Fleet, M.E., Liu, X., Pan, Y., 2000b. Site Preference of Rare Earth Elements in Hydroxyapatite [Ca10(PO4)6(OH)2]. Journal of Solid State Chemistry 149 (2), 391–398.
Garde, A.A., 2002. The Ketilidian orogen of South Greenland: geochronology, tectonics, magmatism, and fore-arc accretion during Palaeoproterozoic oblique convergence. Canadian Journal of Earth Sciences 39 (5), 765–793.
Hamilton, E.I., 1964. The geochemistry of the northern part of the Ilímaussaq intrusion. Meddeleleser om Grønland, SW Greenland, p. 162.
Hansen, E.C., Harlov, D.E., 2007. Whole-rock, Phosphate, and Silicate Compositional Trends across an Amphibolite- to Granulite-facies Transition, Tamil Nadu, India. Journal of Petrology 48 (9), 1641–1680.
Harlov, D.E., 2011. Formation of monazite and xenotime inclusions in fluorapatite megacrysts, Gloserheia Granite Pegmatite, Froland, Bamble Sector, southern Norway. Mineralogy and Petrology 102 (1-4), 77–86.
Harlov, D.E., Förster, H.J., 2003. Fluid-induced nucleation of (Y + REE)-phosphate minerals within apatite: Nature and experiment. Part II. Fluorapatite. American Mineralogist 88 (8-9), 1209–1229.
Harlov, D.E., Wirth, R., Förster, H.J., 2005. An experimental study of dissolution–reprecipitation in fluorapatite: fluid infiltration and the formation of monazite. Contributions to Mineralogy and Petrology 150 (3), 268–286.
Henriksen, N., Higgins, A.K., Kalsbeek, F., Pulvertaft, T.C.R., 2009. Greenland from Archaean to Quaternary, Descriptive text to the 1995 Geological Map of Greenland 1:2 500 000, 2nd edition. Geological Survey of Denmark and Greenland Bulletin 18, 1–126.
Hughes, J.M., Rakovan, J., 2002. The Crystal Structure of Apatite, Ca5(PO4)3(F, OH, Cl). Reviews in Mineralogy and Geochemistry 48 (1), 1–12.
Hughes, J.M., Cameron, M., Mariano, A.N., 1991. Rare-earth element ordering and structural variations in natural rare-earth-bearing apatite. American Mineralogist 76, 1165–1173.
Jacob, D.E., 2006. High sensitivity analysis of trace element poor geological reference glasses by laser-ablation inductively coupled plasma mass spectrometry (LA-ICP-MS). Geostandards and Geoanalytical Research 30, 221–235.
Jochum, K.P., Nohl, U., 2008. Reference materials in geochemistry and environmental research and the GeoReM database. Chemical Geology 253 (1–2), 50–53.
Kempe, U., Götze, J., 2002. Cathodoluminescence (CL) behavior and crystal chemistry of apatite from rare-metal deposits. Mineralogical Magazine 66 (1), 151–172.
Konnerup-Madsen, J., Rose-Hansen, J., 1984. Composition and significance of fluid inclusions in the Ilímaussaq peralkaline granite, South Greenland. Masson 107 (2).
Krumrei, T.V., Pernicka, E., Kaliwoda, M., Markl, G., 2007. Volatiles in a peralkaline system: Abiogenic hydrocarbons and F–Cl–Br systematics in the naujaite of the Ilímaussaq intrusion, South Greenland. Lithos 95 (3–4), 298–314.
Larsen, L.M., 1979. Distribution of REE and other trace elements between phenocrysts and peralkaline undersaturated magmas, exemplified by rocks from the Gardar igneous province, south Greenland. Lithos 12 (4), 303–315.
Larsen, L.M., Sørensen, H., 1987. The Ilímaussaq intrusion-progressive crystallization and formation of layering in an agpaitic magma. Geological Society, London, Special Publications 30 (1), 473–488.

Larsen, L.M., Steenfelt, A., 1974. Alkali loss and retention in an iron-rich peralkaline phonolite dyke from the Gardar province, south Greenland. Lithos 7 (2), 81–90.
Markl, G., Marks, M.A.W., Schwinn, G., Sommer, H., 2001. Phase Equilibrium Constraints on Intensive Crystallization Parameters of the Ilímaussaq Complex, South Greenland. Journal of Petrology 42 (12), 2231–2257.
Marks, M.A.W., Markl, G., 2001. Fractionation and Assimilation Processes in the Alkaline Augite Syenite Unit of the Ilímaussaq Intrusion, South Greenland, as Deduced from Phase Equilibria. Journal of Petrology 42 (10), 1947–1969.
Marks, M.A.W., Markl, G., 2003. Ilímaussaq 'en miniature': closed-system fractionation in an agpaitic dyke rock from the Gardar Province, South Greenland (contribution to the mineralogy of Ilímaussaq no. 117). Mineralogical Magazine 67 (5), 893–919.
Marks, M.A.W., Markl, G., 2015. The Ilímaussaq alkaline complex, South Greenland. In: Charlier, B., Namur, O., Latypov, R., Tegner, C. (Eds.), Layered Intrusions. Springer, Dordrecht (in press).
Marks, M.A.W., Halama, R., Wenzel, T., Markl, G., 2004a. Trace element variations in clinopyroxene and amphibole from alkaline to peralkaline syenites and granites: implications for mineral–melt trace-element partitioning. Chemical Geology 211 (3–4), 185–215.
Marks, M.A.W., Vennemann, T., Siebel, W., Markl, G., 2004b. Nd-, O-, and H-isotopic evidence for complex, closed-system fluid evolution of the peralkaline Ilímaussaq intrusion, South Greenland. Geochimica et Cosmochimica Acta 68, 3379–3395.
Marks, M.A.W., Rudnick, R., Vennemann, T., McCammon, C., Markl, G., 2007. Arrested kinetic Li isotope fractionation at the margin of the Ilímaussaq complex, South Greenland: evidence for open-system processes during final cooling of peralkaline igneous rocks. Chemical Geology 246, 207–230.
Marks, M.A.W., Hettmann, K., Schilling, J., Frost, B.R., Markl, G., 2011. The Mineralogical Diversity of Alkaline Igneous Rocks: Critical Factors for the Transition from Miaskitic to Agpaitic Phase Assemblages. Journal of Petrology 52 (3), 439–455.
Marks, M.A.W., Wenzel, T., Whitehouse, M.J., Loose, M., Zack, T., Barth, M., Worgard, L., Krasz, V., Eby, G.N., Stosnach, H., Markl, G., 2012. The volatile inventory (F, Cl, Br, S, C) of magmatic apatite: An integrated analytical approach. Chemical Geology 291, 241–255.
Noe, D.C., Hughes, J.M., Mariano, A.N., Drexler, J.W., 1993. The crystal structure of monoclinic britholite-(Ce) and britholite-(Y). Zeitschrift für Kristallographie 206, 233–246.
Pan, Y., Fleet, M.E., 2002. Compositions of the Apatite-Group Minerals: Substitution Mechanisms and Controlling Factors. Reviews in Mineralogy and Geochemistry 48 (1), 13–49.
Parsons, I., 2012. Full stop for mother earth. Elements 8, 396–398.
Pasero, M., Kampf, A.R., Ferraris, C.P., Igor, V., Rakovan, J., White, T.J., 2010. Nomenclature of the apatite supergroup minerals. European Journal of Mineralogy 22 (2), 163–179.
Piccoli, P.M., Candela, P.A., 2002. Apatite in Igneous Systems. Reviews in Mineralogy and Geochemistry 48 (1), 255–292.
Poulsen, V., 1964. The sandstones of the Precambrian Eriksfjord formation in South Greenland. GGU.
Rae, A.D., Coulson, M.I., Chambers, D.A., 1996. Metasomatism in the North Qôroq centre, South Greenland: apatite chemistry and rare-earth element transport. Mineralogical Magazine 60, 207–220.
Rakovan, J.F., Reeder, R.J., 1996. Intracrystalline rare earth element distributions in apatite: Surface structural influences on incorporation during growth. Geochimica et Cosmochimica Acta 60 (22), 4435–4445.
Rønsbo, J.G., 1989. Coupled substitutions involving REEs and Na and Si in apatites in alkaline rocks from the Ilímaussaq intrusion, South Greenland, and the petrological implications. American Mineralogist 74, 896–901.
Rønsbo, J.G., 2008. Apatite in the Ilímaussaq alkaline complex: Occurrence, zonation and compositional variation. Lithos 106 (1–2), 71–82.
Schilling, J., Wu, F.-Y., McCammon, C., Wenzel, T., Marks, M.A.W., Pfaff, K., Jacob, D.E., Markl, G., 2011. The compositional variability of eudialyte-group minerals. Mineralogical Magazine 75, 87–115.
Shearer, C., Larsen, L.M., 1994. Sector-zoned aegirine from the Ilímaussaq alkaline intrusion, South Greenland; implications for trace-element behavior in pyroxene. American Mineralogist 79 (3-4), 340–352.
Shore, M., Fowler, A.D., 1996. Oscillatory zoning in minerals; a common phenomenon. The Canadian Mineralogist 34 (6), 1111–1126.
Sørensen, H., 2001. The Ilímaussaq alkaline complex, South Greenland: status of mineralogical research with new results. Geology of Greenland Survey Bulletin, Contributions to the mineralogy of IlímaussaqAnniversary volume with list of minerals. H. Sørensen. København no. 100 p. 190.
Sørensen, H., Bohse, H., Bailey, J.C., 2006. The origin and mode of emplacement of lujavrites in the Ilímaussaq alkaline complex, South Greenland. Lithos 91 (1–4), 286–300.
Sørensen, H., Bailey, J.C., Rose-Hansen, J., 2011. The emplacement and crystallization of the U–Th–REE-rich agpaitic and hyperagpaitic lujavrites at Kvanefjeld, Ilímaussaq alkaline complex, South Greenland. Bulletin of the Geological Society of Denmark 59, 69–92.
Stormer, J.C., 1993. Variation of F and Cl X-ray intensity due to anisotropic diffusion in apatite during electron microprobe analysis. American Mineralogist 78 (5-6), 641–648.
Upton, B.G.J., 2003. Magmatism of the mid-Proterozoic Gardar Province, South Greenland: chronology, petrogenesis and geological setting. Lithos 68 (1–2), 43–65.
Upton, B.G.J., 2013. Tectono-magmatic evolution of the southern branch of the Gardar Rift in the late Gardar Period. Geological Survey of Denmark and Greenland Bulletin 29 (124 pp.).
Ussing, N.V., 1912. Geology of the Country around Julianehåb, Greenland. Meddelelser om Grønland.
van Hinsberg, V.J., Schumacher, J.C., 2007. Intersector element partitioning in tourmaline: a potentially powerful single crystal thermometer. Contributions to Mineralogy and Petrology 153 (3), 289–301.
Wang, L.-X., Marks, M.A.W., Wenzel, T., von der Handt, A., Keller, J., Teiber, H., Markl, G., 2014. Apatites from the Kaiserstuhl Volcanic Complex, Germany: new constraints on the petrogenetic relationship between carbonatite and associated silicate rocks. European Journal of Mineralogy 26, 397–414.
Watson, E.B., Green, T.H., 1981. Apatite/liquid partition coefficients for the rare earth elements and strontium. Earth and Planetary Science Letters 56, 405–421.
Wyllie, P.J., Cox, K.G., Biggar, G.M., 1962. The Habit of Apatite in Synthetic Systems and Igneous Rocks. Journal of Petrology 3 (2), 238–243.

View publication stats